On overtravel and skate in cantilever-based probes for on-wafer measurements

Steve Arscott

On overtravel and skate in cantilever-based probes for on-wafer measurements

Steve Arscott

University of Lille, CNRS, Centrale Lille, Univ. Polytechnique Hauts-de-France, UMR 8520-IEMN, F-59000 Lille, France.

E-mail: steve.arscott@univ-lille.fr

Abstract

Due to the deformability of a microcantilever-based probe, there is an interesting and subtle interplay between the probe overtravel, the tip skate on the surface, and the ultimate tangency of the tip of the probe with the wafer surface. The relationship between these parameters is described here. The scalable model is tested using a macroscopic cantilever and found to be accurate in its predictions. In addition, to avoid potential skate-induced damage to metallisation, the idea of zero-skate using a cantilever-based probe has been introduced; minimal skate is demonstrated using a macroscopic cantilever—the skate can be reduced by a factor of 0.176. As the model is scalable, this information could be of use to the designer of emerging miniature MEMS microcantilever-based surface contact probes destined for on-wafer electrical measurements or the test engineer concerned with on-wafer probe contacting—where skate and overtravel are important practical concerns having repercussions in electrical contact quality. Some predictions of the modelling for microcantilever-based probes are provided.

1. Introduction

Electrical probes are commonplace and employed for all sorts of electrical testing across the world—they are used for on-wafer measurements from DC to microwave frequencies and even beyond [1–3]. When such probes are brought into contact with a metal pad on a chip surface, an extra vertical probe displacement is used to create a low resistance 'metal-to-metal' electrical contact, requiring a certain contact force [4]—this vertical displacement is called the 'overtravel' of the probe. For an angled probe, the overtravel causes a horizontal movement of the probe tip across the metal pad on the underlying chip—this is known as the probe 'skate'. Despite being necessary for a good metal-to-metal electrical contact, excessive probe skate can result in damage to both the probe tip metallization and

the contact pad on the chip—it can also result in an increase in parasitic circuit elements in high frequency measurements. Probe skate is sometimes used beneficially by the microwave test engineer to achieve planarity of the probes [5]. The relationship between overtravel and skate, and the impact of skate on measurements using probes, remains somewhat qualitative in both scientific literature and commercial documentation—with anecdotal 'rules of thumb' common amongst test engineers. Strid [6] first pointed out that the overtravel-to-skate ratio of a probe can be modified by tilting the substrate with respect to the probe. Stephens et al [7] observed that excessive probe skate can be problematic in microwave measurements. Weikel et al [8] noted the problem of large skate in micromachined probes—observing a skate of ~10 μm. Daffe et al [9] pointed out the issue of skate and contact force in silicon microcantilever-based probes for on-wafer measurements—noting that small skate (~1 μm) is achieved using small probes. Wartenburg [2] demonstrated the impact of excessive probe skating on electrical parasitic elements in microwave measurements—a 50 μm skate tripling the series inductance of a pad. Aguilera and Berenguer [10] give typical skate values between 20-45 μm for on-wafer measurements on different pad metals—however, no overtravel is given. More recently, Sakamaki et al [11,12] pointed out the importance of probe skate in the accuracy of the calibration of on-wafer microwave measurements. An accurate control of pad skate via the precise imposition of overtravel is important in the reproducibility of on-wafer RF measurements—much commercial documentation makes a note of this and gives typical values for the test engineer. The overtravel-to-skate ratio is commonly given in the technical documentation of commercial coplanar microwave on-wafer probes; much of the documentation quotes an overtravel-to-skate ratio of 2.5 for an overtravel range of 50-75 μm, e.g. the InfinityXT probe by Cascade Microtech., USA. If we consider the probes to be rigid and only deformable at the probe base/holder—as is the case of some macroscopic probes, then the relationship between the overtravel and the skate is trivial, depending only on the probe's tilt angle. For a given probe angle—usually relatively shallow: 20° to 40°—this ratio is often given in the probe's specifications. The engineer thus applies enough overtravel to achieve an optimum electrical contact whilst hopefully minimizing skate and potential damage to both probe and chip pad. This action enables the probe lifetime to be maximized—such probes can be notoriously expensive—and enables repeated measurements on the same chip pad.

In contrast, the overtravel-to-skate relationship is different and somewhat subtler for microcantilever-based surface contact probes [13–15]. The reason for this is that a microcantilever-based probe, e.g. one based on a silicon microcantilever having lithographically-patterned metal electrical contacts, is mechanically deformable. The geometric relationship between the overtravel, the skate, the contact force, and the tip/surface contact tangency condition is therefore less trivial than for a rigid macroscopic probe counterpart. The microcantilever remains straight upon initial

surface contacting—however, the imposition of overtravel results now in bending of the microcantilever, along with associated skate of the tip on the chip pad. The contact force is thus described by the microcantilever bending and stiffness—the latter governed by the microcantilever's dimensions and material's physical properties. Further bending of the microcantilever eventually leads to a tip/surface tangency condition not observed in macroscopic probes—this eventuality may be of some use to the engineer as it means that small contact pads at the microcantilever tip are now parallel to the chip pad surface—implying a maximum metal-to-metal contact surface. However, as we shall see, given the probe's stiffness, this tangency condition may only be obtained at high contact force and relatively large skate in some cases—something which may cause damage to the probe metallization and the chip pad metallization. Finally, depending on the bending and the stiffness of the microcantilever, a mechanical stress will be generated in the microcantilever—this will have a maximum at the surface of the microcantilever at its fixed end. A probe designer requires knowledge of this stress so as not to exceed the yield strength of the microcantilever material, thus avoiding catastrophic failure.

In the following I will use simple modelling based on some assumptions to describe the interaction between the overtravel, the skate, the contact force, the mechanical stress, and the tangency in microcantilever-based probes. It will also be shown that zero-skate can be achieved for a cantilever-based probe by correct orientation and control of the overtravel direction.

2. Modelling

2.1 The meaning of overtravel and skate in rigid and cantilever-based probes.

Let us first define what we mean by the terms overtravel and skate in the context of both rigid and deformable cantilever-based probes. We can do this best with the help of an illustration—see Figure 1.

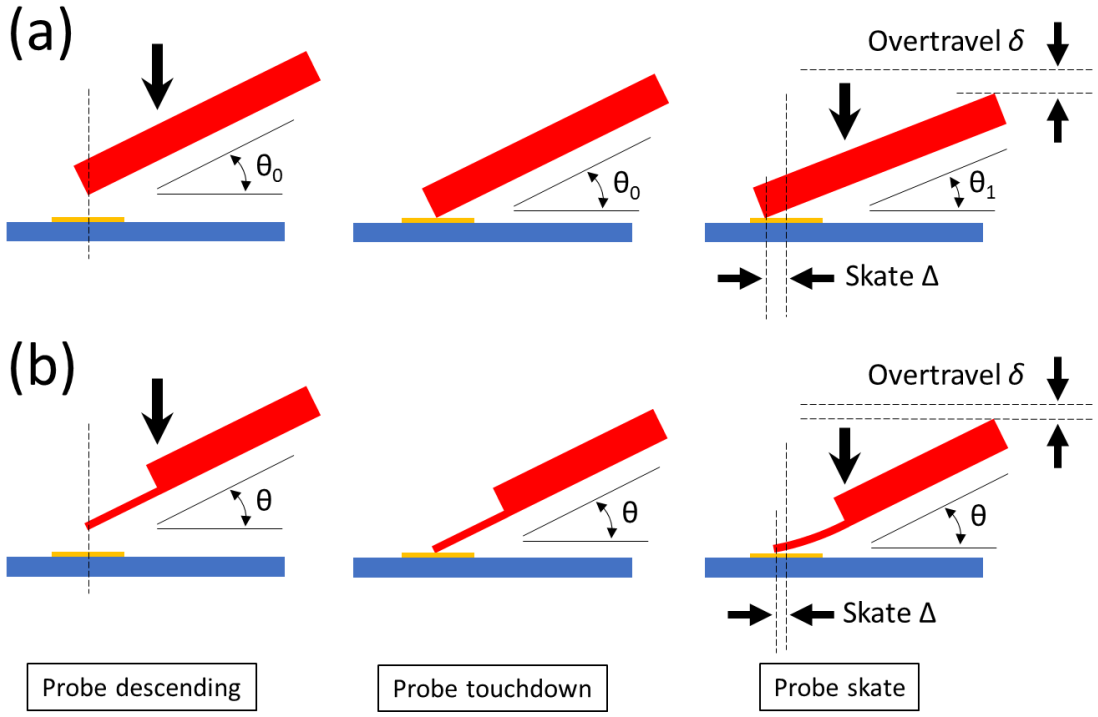

Figure 1. The meaning of overtravel and skate in (a) a rigid probe and (b) a cantilever-based probe.

Overtravel (denoted here by δ) is the extra vertical displacement of the probe holder once the probe tip has made initial contact with the surface (the situation commonly referred to as 'probe touchdown'). The skate (denoted here as Δ) is the horizontal distance travelled by the probe tip for a given vertical overtravel displacement. For a rigid probe, the skate is the result of the whole probe pivoting to modify the probe angle—see Figure 1(a). Unlike the case of the rigid probe, it is evident that the bending of the cantilever must be considered for skate and overtravel in a cantilever-based probe—see Figure 1(b). Note that the probe angle θ remains constant for a cantilever-based probe.

2.2 Skate versus overtravel for a rigid probe

The geometry of the rigid probe shown in Figure 1(a) is illustrated in Figure 2.

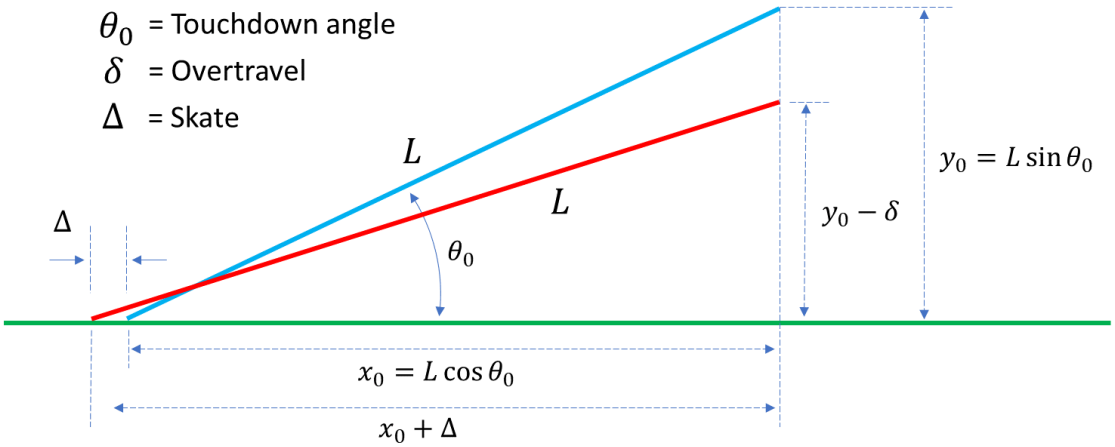

Figure 2. The geometry of the overtravel and the skate of a rigid probe. Probe touchdown (blue) and a skate produced by an overtravel (red).

Elementary trigonometry tells us the tip skate Δ is given by the following formula:

$$\Delta = \sqrt{L^2 - (L \sin\theta_0 - \delta)^2} - L \cos\theta_0 \tag{1}$$

Where L is the length of the probe, δ is the overtravel, and θ_0 is the probe angle at touchdown. As the overtravel increases, the probe angle reduces, i.e. $\theta_1 < \theta_0$. This enables the tip skate and the overtravel-to-skate ratio to be plotted as a function of overtravel for a rigid probe functioning as in Fig. 1(a)—this is shown in Figure 3.

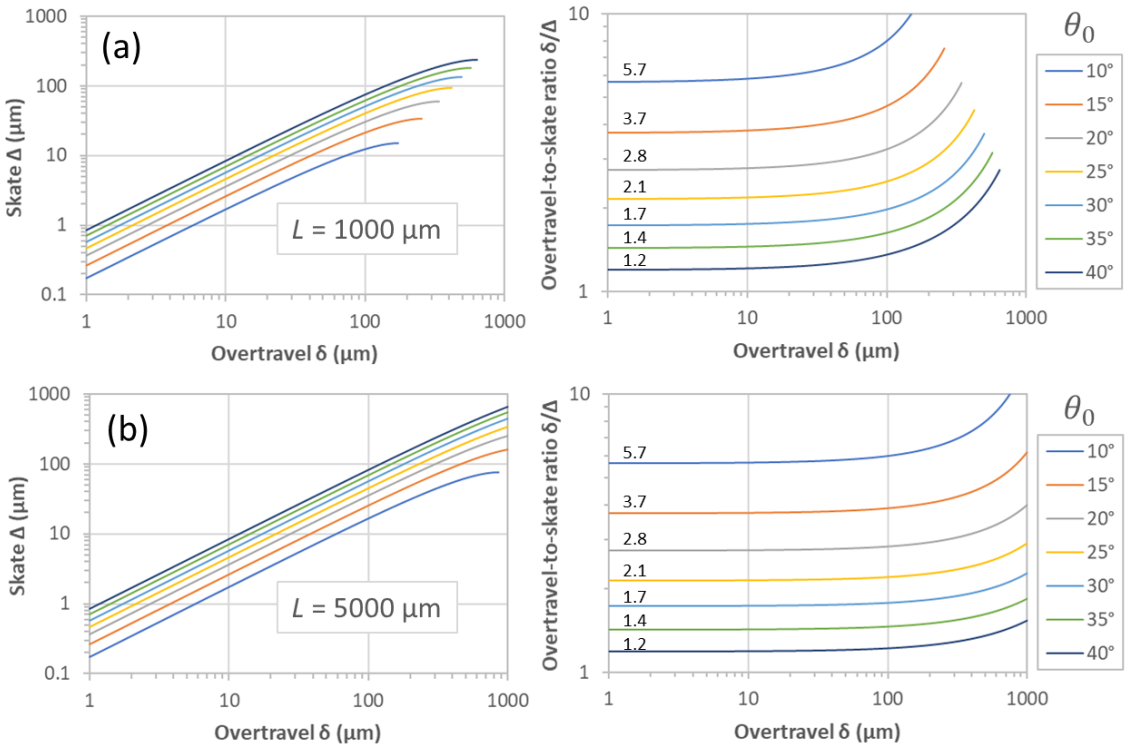

Figure 3. Skate and overtravel in a long rigid probe as a function of touchdown probe angle and probe length. The probe length L equals (a) 1000 μm and (b) 5000 μm, the touchdown angle θ_0 is varied between 10-40°.

Strid [6] measured a skate of 1 mil (25.4 μm) for an overtravel of 5 mils (127 μm) for a wafer tilted at 11.3°; the length of the probe was not given. However, for long probe, Eq. 1 successfully predicts this skate. Commercial macroscopic probes quote an overtravel-to-skate ratio of 2.5—this condition is met for a long probe with a touchdown angle of between 20-25°—the yellow line in Fig. 3(b). Evidently for this type of probe, a lower touchdown angle results in a lower skate for a given overtravel.

2.3 Overtravel and skate in cantilever-based probes

Let us now consider the subtler case of the deformable cantilever-based probe shown in Fig. 1(b) in more detail. Figure 4 shows geometrically the effect of an imposed vertical overtravel on the bending of the cantilever—which results in horizontal skate of the tip on the surface.

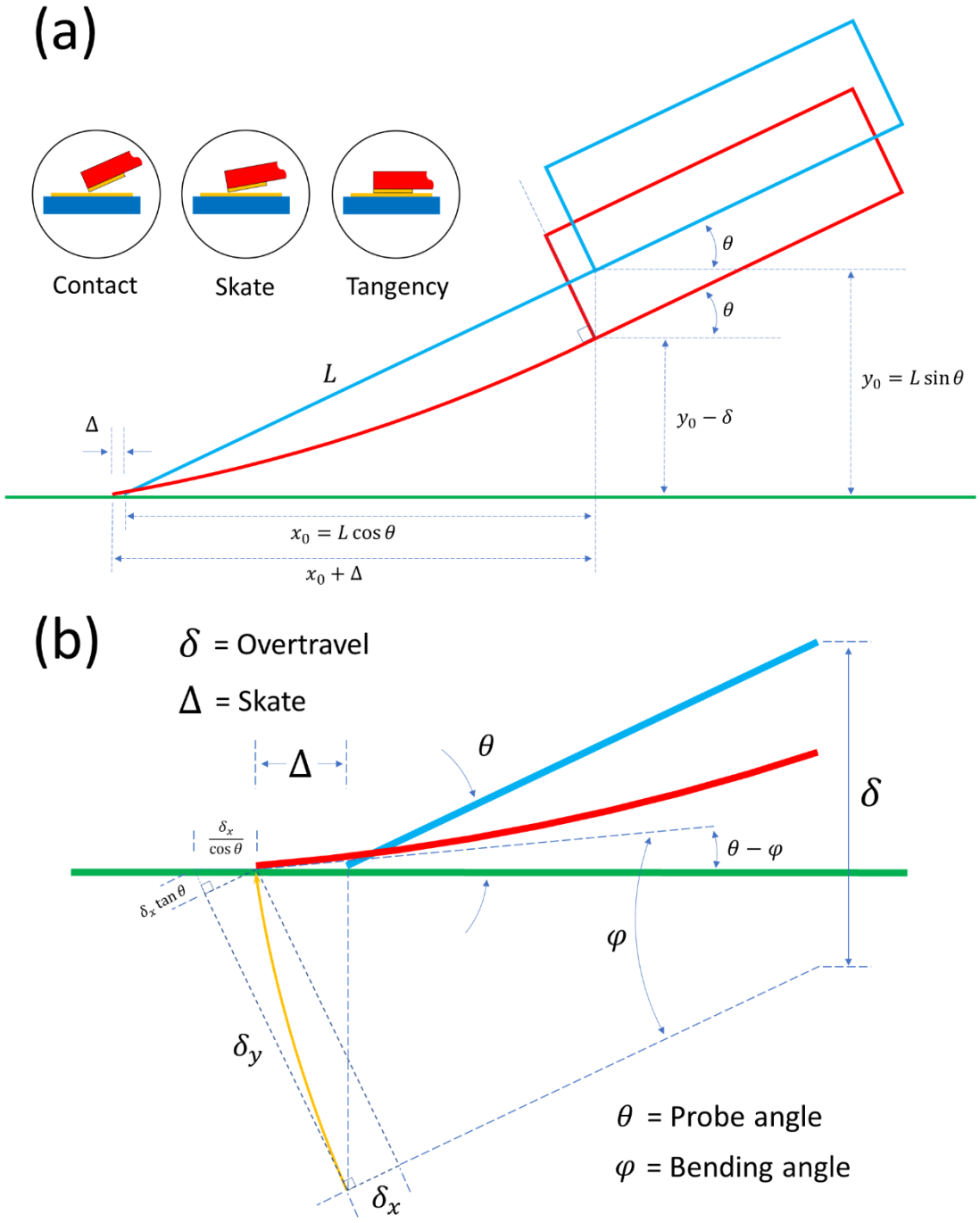

Figure 4. The geometry of the bending of the cantilever due to an imposed overtravel. (a) The blue outline shows the probe (cantilever and rigid support) at tip/surface contact (zero overtravel). The red outline shows the probe bending and skating when an overtravel δ is imposed. The inset in (a) shows the tip/surface cases of contact, skate, and tangency when a practical contact probe pad is considered. (b) A zoom showing the geometry at the tip. The blue outline shows tip/surface contact (zero overtravel). The red outline shows the cantilever bending and the subsequent skate Δ of the tip along the surface (green). The yellow arrowed arc indicates the movement of the cantilever tip in this frame of reference, i.e. with the cantilever tilted to an angle θ.

To derive a formula for the horizontal skate Δ along the surface in terms of the imposed vertical overtravel δ we can consider the geometry of the deflecting fixed-free cantilever illustrated in Fig. 4(b). Elementary trigonometry allows one to obtain the following formulae for the skate Δ in terms of the overtravel δ and the probe angle θ:

$$\Delta = \delta \tan\theta - \frac{\delta_x}{\cos\theta} \tag{2}$$

$$\delta = \delta_y \cos\theta + \delta_x \sin\theta \tag{3}$$

where δ_x and δ_y are the movement of the end of the cantilever as indicated in Fig. 4(b). We therefore require a function describing the geometric relationship between the lateral movement of the end of the cantilever δ_x and the deflection δ_y—as indicated in Fig 4(b). Note that for the moment no force (loading) needs to be considered.

The lateral movement δ_x of the tip of a fixed-free rectangular cantilever beam with a concentrated load at the free end under both small and large deflection [16,17] can be approximated by the following formula:

$$\delta_x = fL\left(1 - \sqrt{\frac{\sin\varphi}{\varphi}}\right) \tag{4}$$

where f is a constant and φ is the rotation angle of the cantilever (with respect to the cantilever support) which is given by:

$$\varphi = \frac{3\delta_y}{2L} \tag{5}$$

The author has explored the validity of these relationships experimentally—see experimental Section 3 and Supplementary Information. For a long, thin cantilever, i.e., $L \gg w$, equations (4) and (5) describe a fixed-free cantilever's lateral deflection accurately for deflections up to $L/3$. For a fixed-free cantilever bending under a concentrated load located at the free end, the following conditions indicate the linear and nonlinear behaviours: $\varphi/\sin\varphi \cong 1$ (linear) and $\varphi/\sin\varphi \gg 1$ (nonlinear)—where φ is the bending angle of the end of the cantilever. Substituting $\delta_y = L/3$ into Eq. (5) gives $\varphi/\sin\varphi = 1.04$.

2.4 Tip/surface contact tangency condition

Following on from the above reasoning, the condition for tangency of the tip of the cantilever with respect to the surface is obtained when the rotation angle of the cantilever equals the probe angle, i.e., $\varphi = \theta$; this occurs for a tangency overtravel δ_T given by:

$$\delta_T = \frac{2L\theta}{3}\cos\theta + fL\sin\theta\left(1 - \sqrt{\frac{\sin\theta}{\theta}}\right) \tag{6}$$

and results in a tangency skate Δ_T equal to:

$$\Delta_T = \delta_T \tan\theta - \frac{fL}{\cos\theta}\left(1 - \sqrt{\frac{\sin\theta}{\theta}}\right) \tag{7}$$

Interestingly, the *tangency* overtravel-to-skate ratio (δ_T/Δ_T) is independent of the cantilever length L and is only a function of the probe angle θ:

$$\frac{\delta_T}{\Delta_T} = \frac{\alpha}{\alpha\beta+\gamma} \tag{8}$$

where

$$\alpha = \frac{2\theta}{3}\cos\theta + f\sin\theta\left(1 - \sqrt{\frac{\sin\theta}{\theta}}\right) \tag{9}$$

$$\beta = \tan\theta \tag{10}$$

$$\gamma = \frac{f}{\cos\theta}\left(1 - \sqrt{\frac{\sin\theta}{\theta}}\right) \tag{11}$$

2.5 Tip/surface contact force variation

As has been stated, a prediction of the tip/surface contact force is important for cantilever-based electrical probes as the contact force governs the electrical contact resistivity of the metal-to-metal contact.

Compared to the overtravel versus skate relationship in Section 2.3, the situation is different when calculating contact force. The well-known linear expressions describing the force and stress in terms of deflection apply if $\varphi/\sin\varphi \cong 1$. However, if $\varphi/\sin\varphi \gg 1$ then we have two options. Either one seeks a solution to the nonlinear problem which describe the force in terms of high deflection [16–24], or one estimates the force and stress using the linear approximation and one applies an error factor based on experimental findings. This last approach has been experimentally investigated in the Supplementary Information.

In the case where $\varphi \cong \sin\varphi$, then the contact force is proportional to the deflection. For a fixed-free rectangular cantilever with a concentrated load at the end of the beam, the contact force F_c at the cantilever/surface point is given by [25]:

$$F_c = \frac{\delta_y E w t^3}{4L^3} \tag{12}$$

In terms of the rotation angle of the cantilever, F_c can be written as:

$$F_c = \frac{\varphi E w t^3}{6L^2} \tag{13}$$

With reference to Figure 4(b), the contact force normal to the surface $F_c^{\perp}$ is thus given by:

$$F_c^{\perp} = \frac{\varphi \cos\theta E w t^3}{6L^2} \tag{14}$$

Therefore, the contact force normal to the surface *when the tip is in tangency with the surface* $F_{cT}^{\perp}$ is given by:

$$F_{cT}^{\perp} = \frac{\theta \cos\theta E w t^3}{6L^2} \tag{15}$$

Note that this model assumes that elementary beam theory is valid; although this may not be the case at very high overtravel—see Supplementary Information for discussion. Notably, for large loads concentrated at the cantilever end, elementary beam theory predicts deflections greater than the length of the beam [18]. This means that in practice if a high deflection is *imposed* on a cantilever (as is the case of imposed overtravel of a probe) then the concentrated load force at the cantilever end is larger than that which is predicted by elementary beam theory—see Supplementary Information. Therefore, if $\varphi \gg \sin\varphi$ (something which becomes apparent for bending angles larger than 30°) then an expression for the force in terms of the cantilever deflection needs to be sought in non-linear approaches to high deflection of a cantilever [16–24]. Section 3 and the Supplementary Information explores the validation of Eq. 13.

2.6 The importance of friction coefficient on skate

In a rigid probe, the overtravel imposes the skate. In contrast, in a cantilever-based probe friction may prevent skate. In this case, the imposition of overtravel would lead to a buckling of the cantilever rather than a skating of the tip on the surface with a quasi-parabolic cantilever being maintained. In an effort to estimate the relationship between skate and friction we can make some assumptions to produce a simple model.

Let us consider how the overtravel/skate relationship depends on friction. By making the assumptions that the contact force model is valid in a first approximation and that the friction force is proportional to the normal contact force in a first approximation one can predict if skate occurs for a specific metal-to-metal probe/surface combination. In this case we are considering the friction

between a small metal pad located at the tip of the cantilever and a metal surface—as shown in the inset to Figure 4(a).

The friction force F_f exerted by a surface when an object moves across is given by:

$$F_f = \mu F_n \tag{16}$$

Where μ is the coefficient of friction between the two materials (static or kinetic) and F_n is the normal force between the materials. From equation 14, the normal force $F_n = F_c^{\perp}$. With reference to Figure 4(b) the contact force parallel to the surface $F_c^{\parallel}$ is given by:

$$F_c^{\parallel} = \frac{\varphi \sin\theta E w t^3}{6L^2} \tag{17}$$

Skate occurs when $F_c^{\parallel} \geq F_f$, this occurs when the following inequality is satisfied:

$$\tan\theta \geq \mu \tag{18}$$

Note that this is the same inequality as for a sliding mass on a slope [26,27], where μ is the static coefficient of friction in this case. Note that Equation 18 implies that in any modelling of skate and overtravel, a small static coefficient of friction is necessary between the materials for the modelling to be valid at low probe angle. It should be noted that the analysis here is a first approximation—for a given materials and surface topographic combination beyond the simple metal-to-metal contact and associated friction coefficient considered here, the role of friction in the forced skating of a small probe tip over a surface is not trivial [28], such as stick-slip behaviour in atomic force microscopy probes [29].

2.7 Stress variation at the fixed end of the cantilever

The stress σ at the surface of the fixed end of the cantilever is given by [25]:

$$\sigma = \frac{\varphi E t}{L} \tag{19}$$

As the overtravel δ is increased, this stress must not exceed the yield strength of the material—otherwise mechanical failure will ensue.

The stress at the surface of the fixed end of the cantilever *when the tip of the cantilever is tangent to the surface* σ_T is given by:

$$\sigma_T = \frac{\theta E t}{L} \tag{20}$$

These two last equations are useful to the probe designer to indicate the potential mechanical failure of the probe or if the tangency condition is possible given the dimensions of the cantilever and the mechanical properties. Note that, as with the contact force calculation, this model assumes a linear elementary beam theory behaviour, i.e. $\varphi \cong \sin\varphi$; this may not be the case at very high overtravel—see Supplementary Information for discussion.

2.8 Achieving zero skate

There are advantages to having zero (or at least minimal) skate: probe tips can be accurately placed, pad damage is reduced, probe damage can be reduced, and pad size can be reduced. As we shall see, the skate could—at least in principle—be avoided using a cantilever setup. Figure 5 illustrates how zero-skate could be achieved for cantilever-based probes.

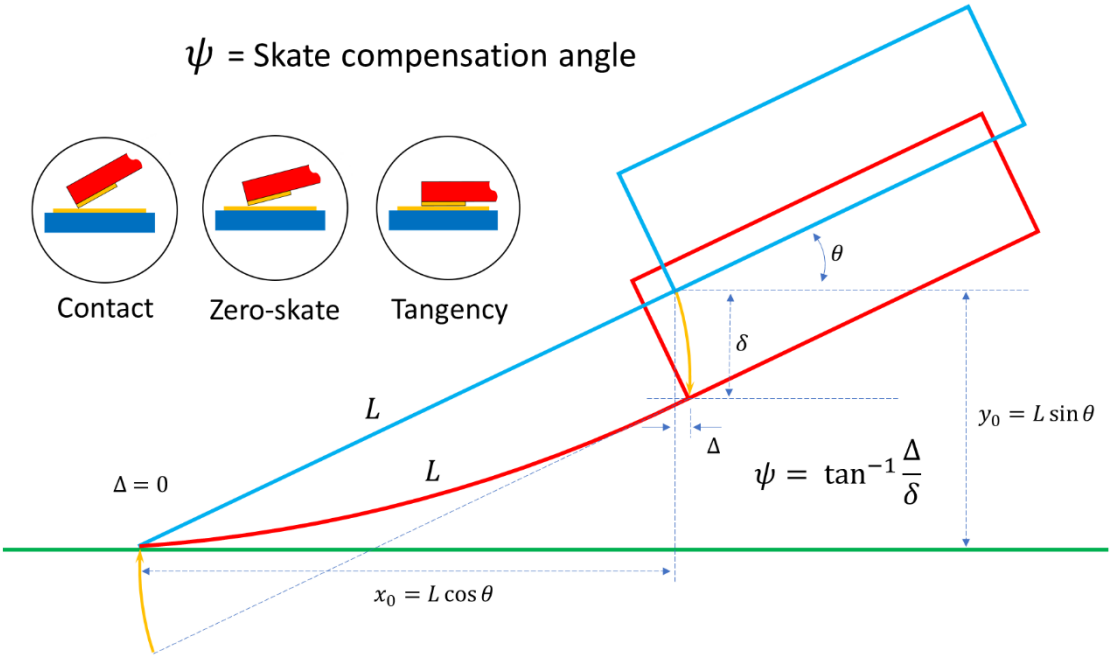

Figure 5. Schematic diagram how zero-skate could be achieved in a cantilever-based probe. Instead of a vertical overtravel, a curved overtravel is used to achieve zero-skate (yellow arcs). For a minimum skate using a linear overtravel, orientating the overtravel direction at an angle ψ is required.

To achieve zero-skate, the probe support would need to be moved down not vertically but in a way that follows the yellow arc illustrated in Figure 5—this is a 180° rotation of the tip trajectory

(also shown at the tip in Fig. 5). This could be achieved practically using a combination of programmed stepper motors for example. However, reduced skate of the tip could be achieved by moving the probe down linearly at a constant 'skate compensation angle' ψ given by:

$$\psi = \tan^{-1}\frac{\Delta_T}{\delta_T} \tag{21}$$

The skate compensation angle and the skate compensation factor are traced as a function of probe angle in Figure 6.

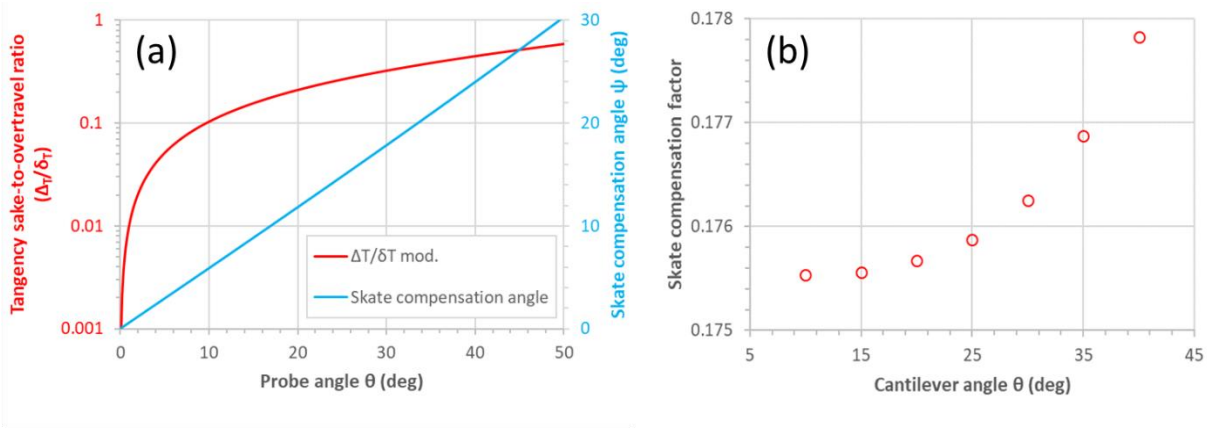

Figure 6. (a) The skate-to-overtravel ratio at tangency and skate compensation angle as a function of probe angle and (b) the sake compensation factor when using a linear angled overtravel at an angle of ψ.

For example, for a typical probe angle of 25° the probe support can be overtravelled down at an angle of ~14.8° to the vertical to achieve minimal skate of the tip of the probe on the surface.

The skate Δ_ψ using a skate compensation angle is thus given by:

$$\Delta_\psi = \Delta - \delta \tan\psi \tag{22}$$

where Δ is the uncompensated skate and δ is the vertical overtravel.

3. Experimental validation of the model using a macroscopic cantilever

Although evidently feasible, the characterization of the skate of a microcantilever appears to be challenging [9]. As the model developed here is—at least in principle—valid at different length scales,

it is simpler first to characterize the skate of a macroscopic cantilever and compare these results with the predictions of the model.

3.1 Validation of Equation 4 using a macroscopic cantilever.

First let us determine the constant f in Equation 4 with the use of a macroscopic cantilever. To do this, a 50 cm long steel ruler (Dextor, France) was employed. The ruler was 2.9 cm wide and 684±1.9 μm thick, i.e. $L \gg w \gg t$. Three cantilever lengths were employed for the experiments: 35 cm, 40 cm, and 45 cm corresponding to a cantilever weight of 51.3 g, 58.6 g, and 65.9 g. In a vertical configuration, the maximum bending for a uniform load (gravity) [25] would be 1.8 cm, 3.3 cm, and 5.4 cm—implying that a horizontal setup is advantageous to avoid bending and bowing; these values compare well with the experimentally obtained values—see Supplementary Information. The ruler was thus clamped and mounted horizontally, rather than vertically, to avoid bending and bowing due to gravity. The experimental setup can be found in the Supplementary Information.

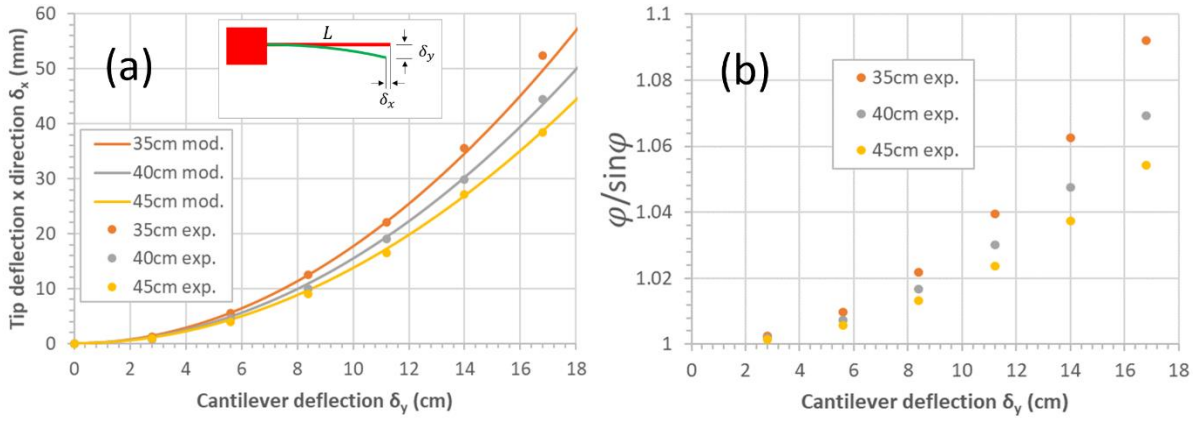

Figure 7. (a) Experimental plots of the cantilever tip deflection in the x-direction δ_x as a function of cantilever deflection δ_y (closed symbols). Three cantilever lengths are used: L = 35 cm, 40 cm, and 45 cm. The inset shows the vertical deflection δ_y and the horizontal deflection δ_x of the tip of the cantilever. The solid lines are obtained by using Equation 4. (b) The ratio $\varphi/\sin\varphi$ plotted as a function of the experimental cantilever deflection δ_y.

Figure 7(a) shows plots of the vertical displacement of the end of the cantilever versus the horizontal displacement of the cantilever for three cantilever lengths: 35 cm, 40 cm, and 45 cm. By tracing Equation 4 in each case, the factor f was determined to be 3.3 over the overtravel range to be

employed in the skate versus overtravel characterization. The model fits the experimental data very well for all three lengths of cantilever. A discrepancy is observed for higher deflections than used here—possibly due to maximum mechanical stress, this will be discussed later. This value of f can be contrasted with values which can be theoretically computed using numerical methods when considering a cantilever deflecting in a perfectly parabolic way. In this case, the theory predicts the value of f in Equation 4 to be equal to 3.577 and 3.675 in the small and large deflection regimes respectively (see Supplementary Information). Figure 7(b) shows the ratio of the cantilever tip angle φ to its sine value plotted against the cantilever deflection in the y direction δ_y. This factor indicates the validity of using the linear approach in the modelling when considering contact force and stress.

3.2 Validation of the model for the overtravel/skate relationship using a macroscopic cantilever.

To characterize the skate versus overtravel relationship, the macroscopic cantilever configuration was used as shown in the setup illustrated in Figure 8.

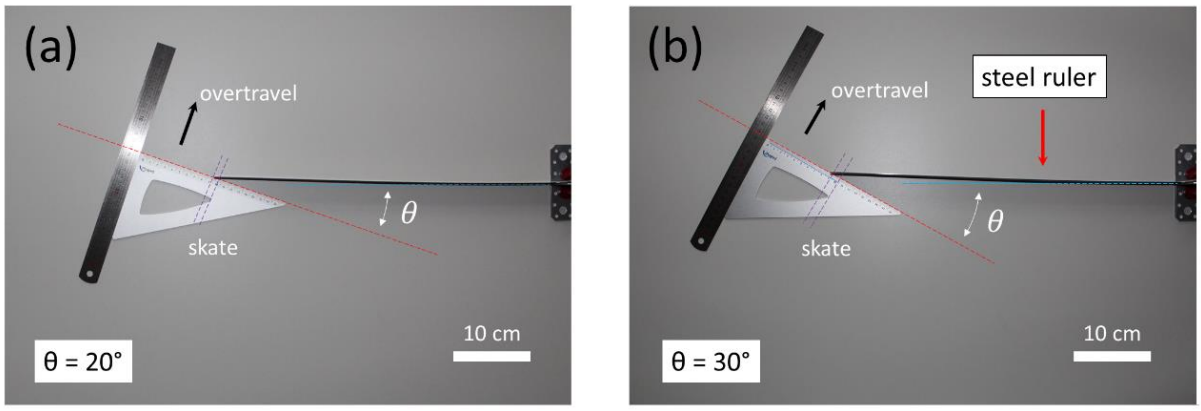

Figure 8. The experimental setup used for the characterization of overtravel and skate for a macroscopic cantilever. A 50 cm long steel ruler is used as the macroscopic cantilever enabling cantilever lengths of 35 cm, 40 cm, and 45 cm orientated at a cantilever angle θ. The overtravel is applied by sliding a set square up a second steel rule—the skate is read off the set square. The overtravel direction is indicated by the black arrows.

Again, a horizontal mounting was employed to avoid bending and bowing of the cantilever due to gravity—as explained above. A second 30 cm long steel ruler and a metal set square were used to simulate the surface and the overtravel. The overtravel was imposed by moving the set square up the

smaller steel ruler and the skate could be read off the set square with an acceptable accuracy of ±0.1 mm using photography—see Supplementary Information.

Figure 9 shows plots of the skate versus the overtravel and the overtravel-to-skate ratio for three cantilevers having a length of 35 cm, 40 cm, and 45 cm for a surface/cantilever angle θ of 10°, 20°, 30°, and 40° (as indicated in Figure 9). The experimental data is shown as open symbols, the solid lines are based on the modelling using the experimentally-determined constant f equal to 3.3.

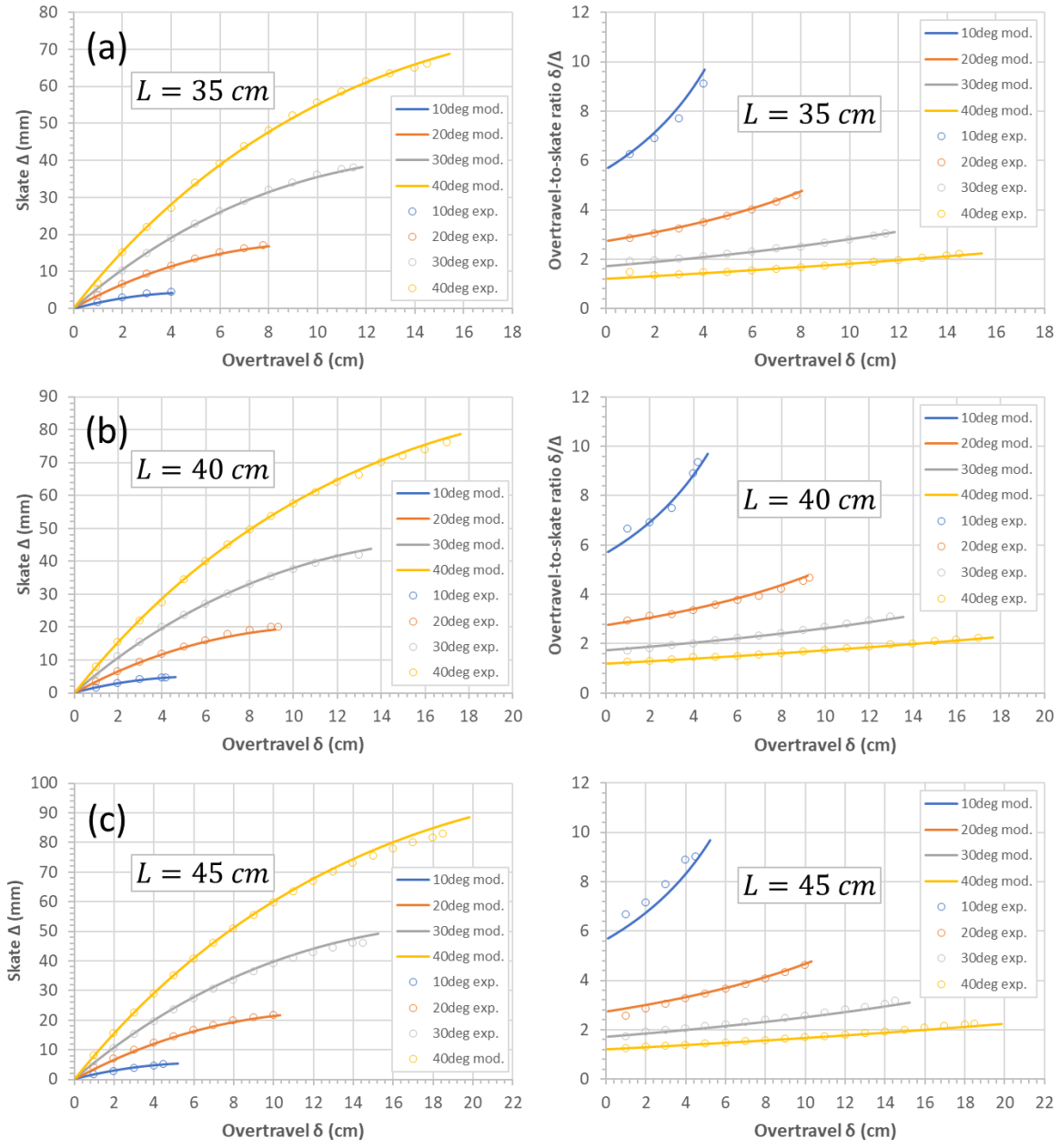

Figure 9. Skate Δ and overtravel-to-skate ratio δ/Δ as a function of overtravel δ for cantilevers having a length L equal to: (a) 35 cm, (b) 40 cm, and (c) 45 cm at different cantilever angles θ. The open symbols are experimentally-obtained values—the solid lines are based on the model developed here. The error on the experimental data points is ±0.1 mm (not shown).

Most of the experimental data agrees quite well with the modelling. There are some discrepancies at small angles and some at high overtravel for the longest cantilever. Theses could be explained by measurement error (see Supplementary Information) and friction (see Section 2.6) or non-linear effects at high deflection—see Supplementary Information for extra results and discussions. The Young's modulus of stainless steel (type 304) is approximately 190 GPa, meaning the cantilever stiffnesses are 10.3 Nm^{-1}, 6.9 Nm^{-1}, and 4.8 Nm^{-1} for a cantilever length of 35 cm, 40 cm, and 45 cm respectively. Note that in the experimental setup, the set square (thickness 1 mm) is in contact with the edge of the end of the steel ruler rather than in the centre of the end of the steel ruler. Such a setup could result in observable twisting of the ruler and an error in the displacement of the tip. However, even in very large deflection >20 cm, the twist was measured and calculated to be <1 mm—this is confirmed by a calculation (see Supplementary Information). The maximum stress at the surface of the fixed end of the cantilever can be calculated for the tangency conditions (see Section 2.7). The tensile yield strength of type 304 steel is ~215 MPa; this is exceeded for two test situations, for a cantilever length of 35 cm (259 MPa) and 40 cm (227 MPa) at an angle of 40°. These measurements were thus performed at the end of the characterization.

Figure 10 shows the experimentally-obtained *tangency* overtravel-to-skate ratio for each length and cantilever angle plotted as a function of angle.

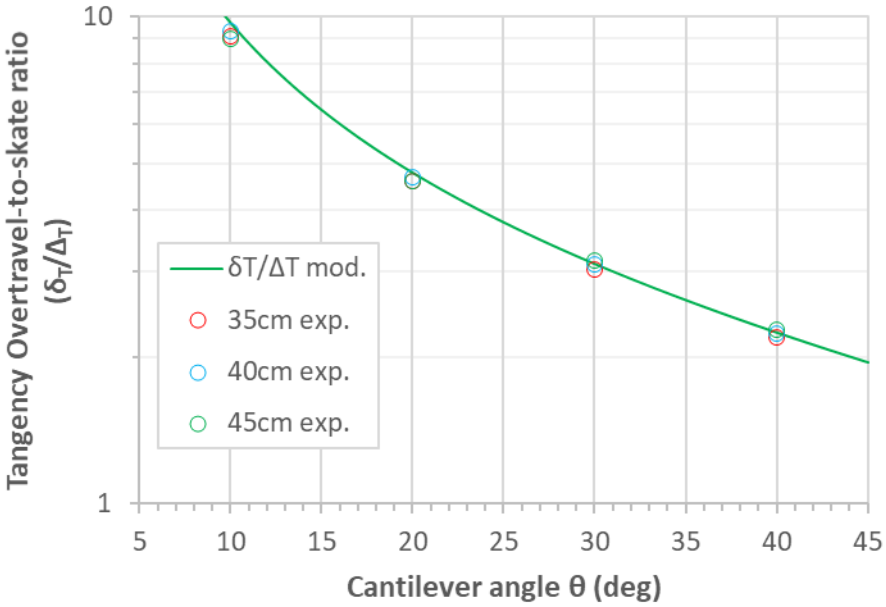

Figure 10. Experimental values of the tangency overtravel-to-skate ratio versus the cantilever angle. The open symbols are the experimentally-obtained values at different cantilever lengths—the green line is the model based on Equation 8. The cantilever lengths L are 35 cm (open red circles), 40 cm (open blue circles), and 45 cm (open green circles).

The model for the tangency overtravel-to-skate ratio given by Equation 8 is also plotted in Fig. 10 as the green curve. The experimentally-obtained values of the tangency overtravel-to-skate ratio agree quite well with the predictions of the modelling—this is especially true for cantilevers angles >10°. In addition, the values of δ_T/Δ_T are very constant when the cantilever length L is varied—as is also predicted by the modelling—see Section 2.4.

3.3 Experimental validation of minimal skate using a 'skate compensation angle' for the overtravel

The macroscopic cantilever can again be used to validate the possibility of reducing skate by the introduction a skate compensation angle ψ to the overtravel direction. This was achieved using the same experimental setup as described above in Figure 8, but this time by introducing some angled mechanical parts into the configuration as shown below in Figure 11.

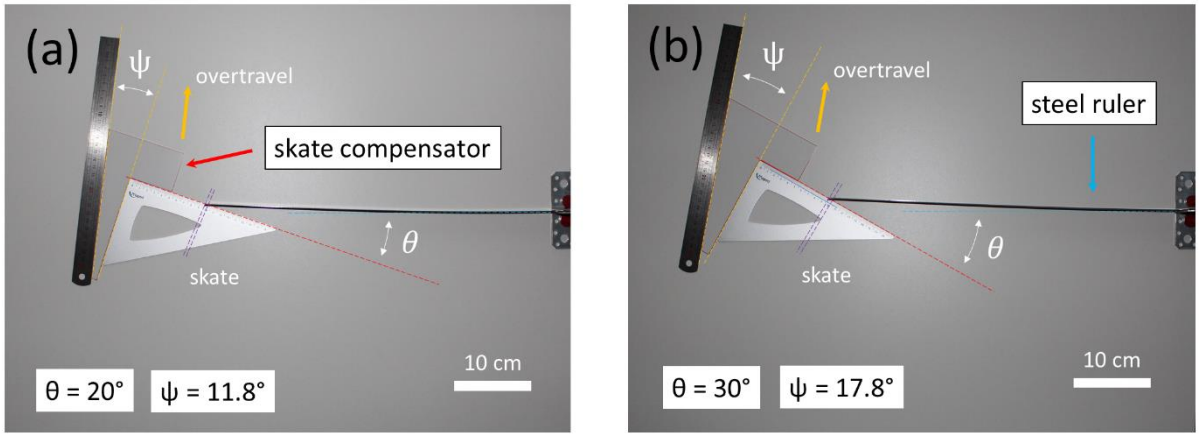

Figure 11. The experimental setup used to validate the possibility of minimal skate by introducing a 'skate compensation angle' ψ into the overtravel direction. This was achieved by specially cut-out mechanical angle parts indicated by the red arrow in (a). The overtravel direction is indicated by the yellow arrows. The experiments were performed at a skate compensation angle equal to (a) 11.8° and (b) 17.8°. The cantilever (steel ruler) is indicated by the blue arrow in (b).

The experiment was conducted using two 1.5 mm-thick in-house fabricated plastic (polystyrene) skate compensation parts ($\psi \cong 12°$ and $\psi \cong 18°$) indicated in the figure—see Supplementary Information. Note that the real vertical overtravel of the cantilever δ is calculated by multiplying the cosine of the skate compensated angle ψ by the inclined overtravel, i.e., $\delta = \delta_\psi \cos\psi$. The direction of the inclined overtravel is indicated in Figure 11 by the yellow arrows.

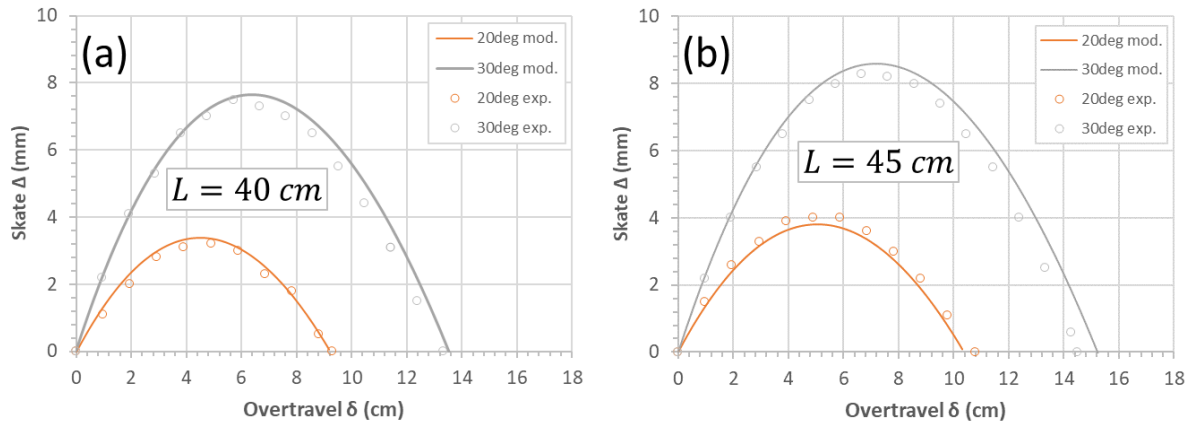

Figure 12. Experimental (symbols) and modelled (curves) skate Δ verses overtravel δ for a cantilever length L of (a) 40 cm and (b) 45 cm. For the modelling, the skate compensation angle ψ is 11.8° and 17.8° for cantilever angles θ of 20° and 30°. The modelled curves are based on Eq. 19.

Figure 12 shows the experimentally-obtained skate (open symbols) verses overtravel for two different cantilever lengths: (a) 40 cm and (b) 45 cm at two different cantilever angles θ. When the skate compensation angle part is included in the experiments, the skate is observed to increase to a maximum and decrease to zero near tip tangency. In this case, the maximum skate is somewhat less than the skate observed for a vertical overtravel. Experimentally, by imposing the skate compensation angle on the overtravel direction the skate can be reduced by a factor of on average 0.176—this is reasonably close to the theoretical value shown in Fig. 6(b). The curves in Fig. 12 are based on the model given in Eq. 19. Note that the maximum skate, when using the skate compensation, is sensitive to the skate compensation angle and therefore the accuracy of the plastic skate compensator—discrepancies between the experimental data points and the modelling in Fig. 12 can be explained by this (see Supplementary Information of and estimation of the experimental error).

4. Some predictions of the model for microcantilevers-based probes

4.1 Overtravel versus skate in microcantilever-based probes

We are now able to make some predictions regarding probe overtravel, tip skate, contact force, and stress by using practical microcantilever dimensions and materials. Crystalline silicon is a very common material used for chip-edge, fixed-free microcantilever fabrication [30]. Microcantilevers are often made using (100) silicon wafers and orientated perpendicularly to the <110> wafer flat—the Young's modulus of silicon in this case is equal to 169 GPa [31]. In terms of mechanical stress, the yield strength of single crystal silicon is of the order of 7 GPa [32]. In terms of dimensions, let us take the cantilever length L to be 400 μm in order to make some predictions as the probe angle varies. The probe angle θ is an interesting practical parameter to study, plots are made from θ = 5° to 35°. Figure 14 shows modelled plots of the skate versus the overtravel and the overtravel-to-skate ratio of a silicon microcantilever as a function of probe angle θ.

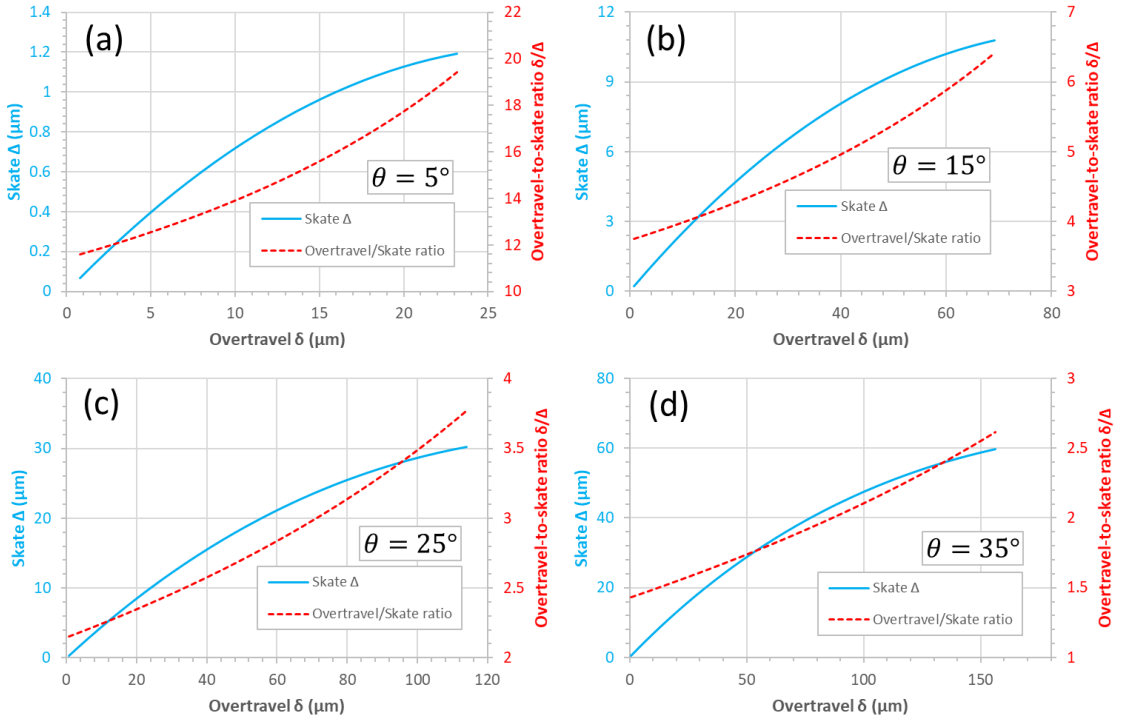

Figure 13. Microcantilever probe Skate Δ and Overtravel-to-skate ratio (δ/Δ) plotted as a function of the overtravel δ for a probe angle θ of (a) 5°, (b) 15°, (c) 25°, and (d) 35°. The length of the silicon microcantilever has a length of 400 μm.

Figure 13 shows that the skate (for a given overtravel) can be reduced greatly if a small probe angle is employed, e.g. if θ = 5°, the skate is submicron for an overtravel <15 μm—see Figure 13(a); although this of course could be at the expense of contact force. In the case of a more common probe angle i.e. θ = 25°, one finds an overtravel-to-skate ratio comparable with those in commercial literature—see Figure 13(c). At higher angles, the skate becomes large for a given overtravel—see Figure 14(d).

4.2 Tip/surface tangency

An interesting situation to consider in microcantilever-based probes is that of tip tangency. This does not occur in rigid probes, except in the case when the probe angle equals zero—see Fig. 1(a). In contrast, for a microcantilever-based probe there will be a certain overtravel whereby the bending of the microcantilever will cause the tip of the microcantilever to be tangent to the wafer surface—this occurs when the bending angle of the microcantilever φ equals the probe angle θ—see Section 2. Let us now see when that happens for microcantilevers having a length of 200 μm, 400 μm, and 800 μm.

Figure 15 shows plots of the skate at tip tangency Δ_T and the overtravel required to achieve tip tangency δ_T as a function of probe angle θ.

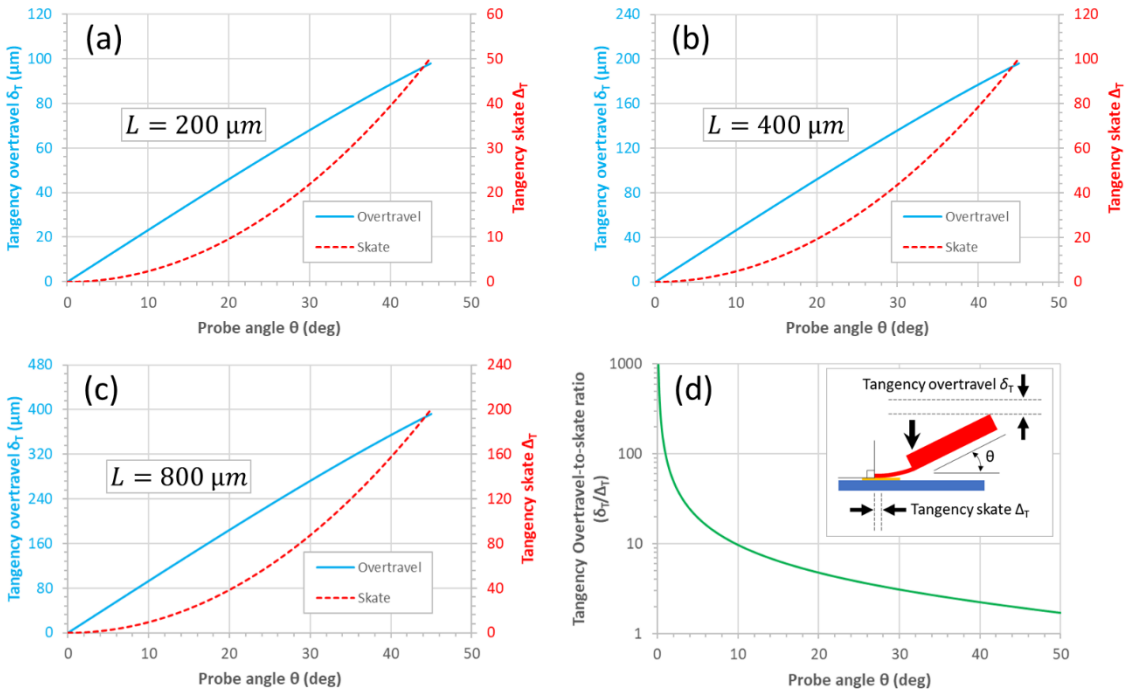

Figure 14. Skate and overtravel at tip tangency in a microcantilever-based probe. The tangency skate Δ_T and the overtravel required for tangency δ_T for a microcantilever length of (a) 200 µm, (b) 400 µm, and (c) 800 µm as a function of probe angle. (d) The overtravel-to-skate ratio at tip tangency as a function of probe angle.

Figure 14 demonstrates clearly that the overall shape of the tangency overtravel and the skate overtravel as a function of probe angle is independent of the probe length—see Figs. 14(a)-(c). This is best seen in Fig. 14(d) which plots the tangency overtravel-to-skate ratio as a function of the probe angle—this is independent of probe length. The inset to Fig. 14(d) shows the tangency condition when sufficient bending due to the overtravel causes the tip of the microcantilever is parallel to the wafer surface.

4.3 Contact force and maximum stress

The contact force and maximum stress are mathematically less interesting than the geometrical aspects of the overtravel/skate relationship. However, as they provide important information

concerning the potential practical performance of the probe (the electrical resistance of a metal-to-metal contacts depends greatly on the contact force [4]) and its mechanical failure, I will plot these with the same probes angles used to plot Fig. 14—this is shown in Figure 15.

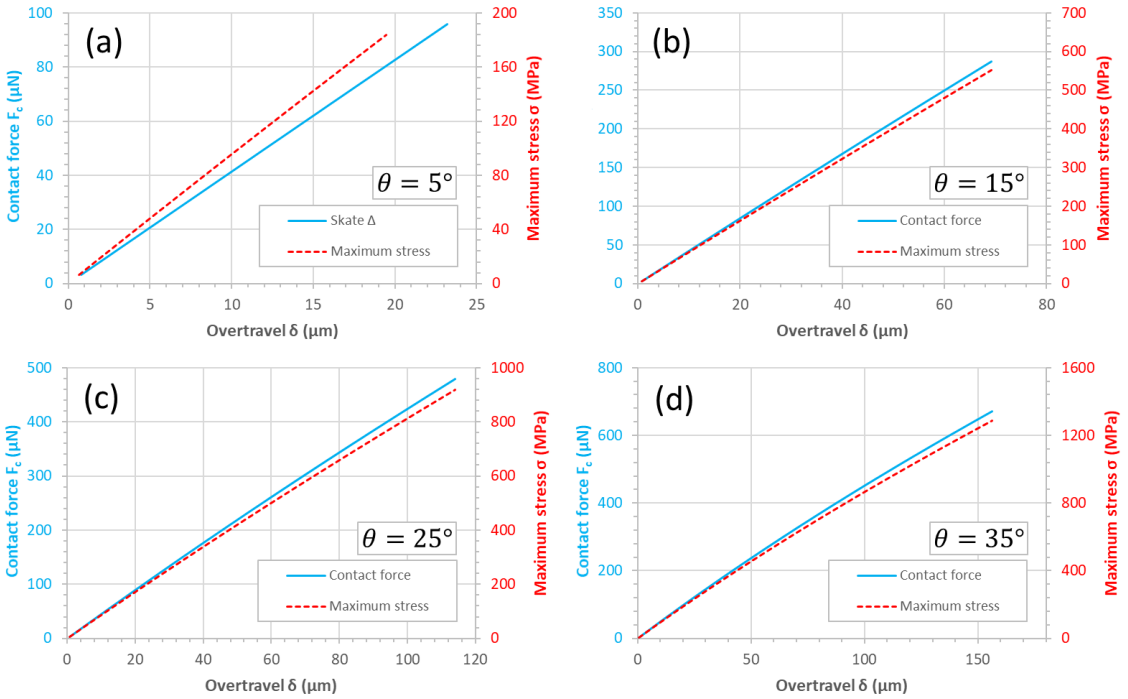

Figure 15. The contact force at the microcantilever tip and the maximum stress at the base of the microcantilever as a function of overtravel for probe angles of (a) 5°, (b) 15°, (c) 25°, and (d) 35°. The length L, the width w and the thickness t of the microcantilever are 400 µm, 50 µm and 5 µm in each case. The stiffness of the cantilever is ~4.1 Nm^{-1}.

In order to verify the predictions concerning microcantilevers, experimentation would need to be required. One could imagine observational experimentation where the overtravel and skate of a microcantilever are observed during scanning electron microscopy. Another approach would be to impose a known overtravel and observe he traces (damage) left on a substrate—as we have previously demonstrated [9].

Finally, a note of caution concerning the calculation of the contact force and the stress at high overtravel. As has been stated, the models given in Section 2 are linear and may not be valid at high tip deflection (large overtravel) [16–24]. Supplementary experiments on the macroscopic cantilevers given in the Supplementary Information indicate that the validity of the modelling of microcantilever here is reasonable up to a tip deflection of ~130 µm. For values of overtravel beyond this, an estimation

of the error in the contact force can be found in the Supplementary Information. For example, for a tip deflection of 160 µm—see Figure 16(d)—the contact force is 1.1 times that computed using the linear model—see the Supplementary Information. Supplementary Figure 11 (see Supplementary Information) can be used to assess the validity of the linear approach.

4.4 Relevance for near-field microscopy probes.

The ideas presented here apply primarily to macroscopic and microscopic electrical probes. In practice, it is well known that such probes require a certain contact force to achieve a minimal contact resistance between the tip and the surface. The imposition of a non-negligible overtravel is required to achieve this tip/surface force—this overtravel results in a certain probe skate due to the deformation of the probe. However, it is interesting to discuss the relevance of the ideas here in the context of microscopic near field probes. First, in terms of near-field probes (for example those used in AFM force spectroscopy), the cantilever deflections are typically small <<100 nm. Using typical values for an AFM probe (t = 2 um, w = 50 µm, L = 450 µm, stiffness = 0.18 N m^{-1}, probe angle θ = 25°) the model computes an overtravel-to-skate ratio of approximately 2 at low deflections. This implies that a cantilever deflection of 10 nm would result—at least in principle—in a tip skate of ~5 nm. Second, near field probes often contain a very sharp point at the tip of the cantilever. In this case, and for small deflections and tip skating, more elaborate modelling of the tip/surface interactions would need to be considered to have a better understanding of the overtravel/skate relationship. Another issue concerning microcantilevers is that the stiffness changes due to a metal coating [33] and can be variable according to fabrication process [34]. Near-field microcantilevers can also have other geometric forms [35,36] beyond the rectangular case considered here [37]. However, the approach could—at least in principle—be extended to other cantilever forms common in near-field microscopy. For a given probe overtravel, the cantilever stiffness governs the tip/surface force and the stress. In the case of practical near-field probes, the stiffness can be obtained using experimentation. A practical calibration of the stiffness of a microcantilever can be performed using various approaches which is independent of the geometric form. Such approaches include: cantilever thermal noise methods [38], reference cantilever methods [39], and dynamic methods [37]. Finally, force calibration methods of AFM tips [40] for contact mode, low deflection AFM studies involves relatively small tip skate—however it is possible that the skate compensation is applicable in the case of large deflection scenarios.

5. Conclusions

By using simple modelling, the relationship between the skate and overtravel of a deformable cantilever-based probe can be described and predicted. Interestingly, the modelling predicts that the ratio between the tangency overtravel and the tangency skate is independent of the microcantilever length—depending only on the probe angle. It is predicted that friction should play a role in probe skating during on-wafer measurements—a simple model is proposed. A macroscopic cantilever can be successfully used to provide experimental data regarding overtravel and skate. The macroscopic cantilever can also be used experimentally to give an idea of the validity range of the modelling when applied to microcantilevers. It was found that for large imposed overtravel (high cantilever deflection) the tip/surface force is larger than that predicted by theory. The experimental data agrees reasonably well with all the predictions of the modelling. The idea of zero-skate using a microcantilever-based probe has been proposed—its experimental proof-of-concept has been experimentally demonstrated using macroscopic cantilever. The modelling and experimental data could be of used to the designer of cantilever-based electrical probes or the test engineer concerned with on-wafer probe contacting where skate and overtravel are important for electrical contacting quality. Some of the ideas may also have relevance in microcantilevers used for contact mode near-field microscopy. An experimental study to reveal the role of friction in the relationship between overtravel and skate in microcantilever-based probes would be interesting.

Data availability statement

The data that support the findings of this study are available upon reasonable request from the authors.

Acknowledgements

The work was partly funded by the French RENATECH network. The author would like to thank Rose Arscott for help with the experimental part of the work.

ORCID iD

Steve Arscott https://orcid.org/0000-0001-9938-2683

References

[1] Strid E 1997 A History of Microwave Wafer Probing *50th ARFTG Conference Digest* 50th ARFTG Conference Digest (Portland, OR, USA: IEEE) pp 27–34

[2] Wartenberg S A 2003 Selected topics in rf coplanar probing *IEEE Trans. Microw. Theory Tech.* **51** 1413–21

[3] Rumiantsev A and Doerner R 2013 RF Probe Technology: History and Selected Topics *IEEE Microw. Mag.* **14** 46–58

[4] Slade P G 2014 *Electrical contacts: principles and applications* (Boca Raton, Fla.: CRC Press)

[5] Wartenberg S 2003 RF coplanar probe basics *Microw. J.* **46** 20–2

[6] Strid E w. 1988 Wideband Probing Techniques For Planar Devices: A Review Semiconductor Conferences ed R K Jain (Bay Point, FL) p 155

[7] Stephens D, Young P R and Robertson I D 2005 Millimeter-wave substrate integrated waveguides and filters in photoimageable thick-film technology *IEEE Trans. Microw. Theory Tech.* **53** 3832–8

[8] Weikle R M, Barker N S, Lichtenberger A W, Bauwens M F and Alijabbari N 2014 Micromachined probes for characterization of terahertz devices *2014 39th International Conference on Infrared, Millimeter, and Terahertz waves (IRMMW-THz)* 2014 39th International Conference on Infrared, Millimeter, and Terahertz waves (IRMMW-THz) (Tucson, AZ, USA: IEEE) pp 1–3

[9] Daffe K, Marzouk J, Boyaval C, Dambrine G, Haddadi K and Arscott S 2022 A comparison of pad metallization in miniaturized microfabricated silicon microcantilever-based wafer probes for low contact force low skate on-wafer measurements *J. Micromechanics Microengineering* **32** 015007

[10] Aguilera J and Berenguer R 2004 *Design and Test of Integrated Inductors for RF Applications* (Boston, MA: Springer US)

[11] Sakamaki R and Horibe M 2019 Uncertainty Analysis Method Including Influence of Probe Alignment on On-Wafer Calibration Process *IEEE Trans. Instrum. Meas.* **68** 1748–55

[12] Sakamaki R and Horibe M 2020 Precision Adjustment of Probe Tilt Angle with RF Signal Detection Technique *IEEE Trans. Instrum. Meas.* 1–1

[13] Reck T J, Chen L, Zhang C, Arsenovic A, Groppi C, Lichtenberger A W, Weikle R M and Barker N S 2011 Micromachined Probes for Submillimeter-Wave On-Wafer Measurements—Part I: Mechanical Design and Characterization *IEEE Trans. Terahertz Sci. Technol.* **1** 349–56

[14] Reck T J, Chen L, Zhang C, Arsenovic A, Groppi C, Lichtenberger A, Weikle R M and Barker N S 2011 Micromachined Probes for Submillimeter-Wave On-Wafer Measurements—Part II: RF Design and Characterization *IEEE Trans. Terahertz Sci. Technol.* **1** 357–63

[15] Marzouk J, Arscott S, Fellahi A E, Haddadi K, Lasri T, Christophe Boyaval and Dambrine G 2015 MEMS probes for on-wafer RF microwave characterization of future microelectronics: design, fabrication and characterization *J Micromech Microeng* **25** 075024

[16] Wang J, Chen J-K and Liao S 2008 An explicit solution of the large deformation of a cantilever beam under point load at the free tip *J. Comput. Appl. Math.* **212** 320–30

[17] Tolou N and Herder J L 2009 A Seminalytical Approach to Large Deflections in Compliant Beams under Point Load *Math. Probl. Eng.* **2009** 1–13

[18] Bisshopp K E and Drucker D C 1945 Large deflection of cantilever beams *Q. Appl. Math.* **3** 272–5

[19] Bisshopp K E 1973 Approximations for large deflection of a cantilever beam *Q. Appl. Math.* **30** 521–6

[20] Beléndez T, Neipp C and Beléndez A 2002 Large and small deflections of a cantilever beam *Eur. J. Phys.* **23** 371–9

[21] Banerjee A, Bhattacharya B and Mallik A K 2008 Large deflection of cantilever beams with geometric non-linearity: Analytical and numerical approaches *Int. J. Non-Linear Mech.* **43** 366–76

[22] Morsch F M, Tolou N and Herder J L 2009 Comparison of Methods for Large Deflection Analysis of a Cantilever Beam Under Free End Point Load Cases *Volume 7: 33rd Mechanisms and Robotics Conference, Parts A and B* ASME 2009 International Design Engineering Technical Conferences and Computers and Information in Engineering Conference (San Diego, California, USA: ASMEDC) pp 183–91

[23] Chen L 2010 An integral approach for large deflection cantilever beams *Int. J. Non-Linear Mech.* **45** 301–5

[24] Tari H 2013 On the parametric large deflection study of Euler–Bernoulli cantilever beams subjected to combined tip point loading *Int. J. Non-Linear Mech.* **49** 90–9

[25] Young W C and Budynas R G 2002 *Roark's formulas for stress and strain* (New York: McGraw-Hill)

[26] Rabinowicz E 1951 The Nature of the Static and Kinetic Coefficients of Friction *J. Appl. Phys.* **22** 1373–9

[27] Blau P J 2009 *Friction science and technology: from concepts to applications* (Boca Raton (Fla.): CRC press)

[28] Ogletree D F, Carpick R W and Salmeron M 1996 Calibration of frictional forces in atomic force microscopy *Rev. Sci. Instrum.* **67** 3298–306

[29] Mate C M, McClelland G M, Erlandsson R and Chiang S 1987 Atomic-Scale Friction of a Tungsten Tip on a Graphite Surface *Scanning Tunneling Microscopy* Perspectives in Condensed Matter Physics vol 6, ed H Neddermeyer (Dordrecht: Springer Netherlands) pp 226–9

[30] Lerond T, Yarekha D, Avramovic V, Mélin T and Arscott S 2021 Surface micromachining of chip-edge silicon microcantilevers using xenon difluoride etching of silicon-on-insulator *J. Micromechanics Microengineering* **31** 085001

[31] Hopcroft M A, Nix W D and Kenny T W 2010 What is the Young's Modulus of Silicon? *J. Microelectromechanical Syst.* **19** 229–38

[32] Petersen K E 1982 Silicon as a mechanical material *Proc. IEEE* **70** 420–57

[33] Sader J E, Larson I, Mulvaney P and White L R 1995 Method for the calibration of atomic force microscope cantilevers *Rev. Sci. Instrum.* **66** 3789–98

[34] Drummond C J and Senden T J 1995 Characterisation of the Mechanical Properties of Thin Film Cantilevers with the Atomic Force Microscope *Mater. Sci. Forum* **189–190** 107–14

[35] Sader J E 1995 Parallel beam approximation for V-shaped atomic force microscope cantilevers *Rev. Sci. Instrum.* **66** 4583–7

[36] Slattery A D, Blanch A J, Shearer C J, Stapleton A J, Goreham R V, Harmer S L, Quinton J S and Gibson C T 2019 Characterisation of the Material and Mechanical Properties of Atomic Force Microscope Cantilevers with a Plan-View Trapezoidal Geometry *Appl. Sci.* **9** 2604

[37] Sader J E, Chon J W M and Mulvaney P 1999 Calibration of rectangular atomic force microscope cantilevers *Rev. Sci. Instrum.* **70** 3967–9

[38] Sader J E, Borgani R, Gibson C T, Haviland D B, Higgins M J, Kilpatrick J I, Lu J, Mulvaney P, Shearer C J, Slattery A D, Thorén P-A, Tran J, Zhang H, Zhang H and Zheng T 2016 A virtual instrument to standardise the calibration of atomic force microscope cantilevers *Rev. Sci. Instrum.* **87** 093711

[39] Slattery A D, Blanch A J, Quinton J S and Gibson C T 2013 Calibration of atomic force microscope cantilevers using standard and inverted static methods assisted by FIB-milled spatial markers *Nanotechnology* **24** 015710

[40] Slattery A D, Blanch A J, Quinton J S and Gibson C T 2013 Accurate measurement of Atomic Force Microscope cantilever deflection excluding tip-surface contact with application to force calibration *Ultramicroscopy* **131** 46–55